Received: 21 April 2021 | Revised: 25 June 2021 | Accepted: 15 July 2021

DOI: 10.1096/fj.202100664R

RESEARCH ARTICLE

THE FASEB JOURNAL

Proteomic analysis of ubiquitination substrates reveals a CTLH E3 ligase complex-dependent regulation of glycolysis

Matthew E. R. Maitland[1,2,3] | **Miljan Kuljanin**[2,3] | **Xu Wang**[1] | **Gilles A. Lajoie**[2,3] | **Caroline Schild-Poulter**[1,2]

[1]Robarts Research Institute, Schulich School of Medicine & Dentistry, Western University, London, ON, Canada

[2]Department of Biochemistry, Schulich School of Medicine & Dentistry, Western University, London, ON, Canada

[3]Don Rix Protein Identification Facility, Schulich School of Medicine & Dentistry, Western University, London, ON, Canada

Correspondence
Caroline Schild-Poulter, Robarts Research Institute, Schulich School of Medicine & Dentistry, Western University, 1151 Richmond Street North, London, ON, N6A 5B7, Canada.
Email: cschild-poulter@robarts.ca

Funding information
Gouvernement du Canada | Canadian Institutes of Health Research (CIHR), Grant/Award Number: MOP-142414; Canada Foundation for Innovation (CFI); Government of Ontario, Grant/Award Number: Ontario graduate Scholarship; Gouvernement du Canada | Natural Sciences and Engineering Research Council of Canada (NSERC), Grant/Award Number: Postgraduate Scholarship-Doctoral (PGS D)

Abstract

Ubiquitination is an essential post-translational modification that regulates protein stability or function. Its substrate specificity is dictated by various E3 ligases. The human C-terminal to LisH (CTLH) complex is a newly discovered multi-subunit really interesting new gene (RING) E3 ligase with only a few known ubiquitination targets. Here, we used mass spectrometry-based proteomic techniques to gain insight into CTLH complex function and ubiquitination substrates in HeLa cells. First, global proteomics determined proteins that were significantly increased, and thus may be substrates targeted for degradation, in cells depleted of CTLH complex member RanBPM. RanBPM-dependent ubiquitination determined using diGLY-enriched proteomics and the endogenous RanBPM interactome further revealed candidate ubiquitination targets. Three glycolysis enzymes alpha-enolase, L-lactate dehydrogenase A chain (LDHA), and pyruvate kinase M1/2 (PKM) had decreased ubiquitin sites in shRanBPM cells and were found associated with RanBPM in the interactome. Reduced polyubiquitination was validated for PKM2 and LDHA in cells depleted of RanBPM and CTLH complex RING domain subunit RMND5A. PKM2 and LDHA protein levels were unchanged, yet their activity was increased in extracts of cells with downregulated RanBPM. Finally, RanBPM deficient cells displayed enhanced glycolysis and deregulated central carbon metabolism. Overall, this study identifies potential CTLH complex ubiquitination substrates and uncovers that the CTLH complex inhibits glycolysis via non-degradative ubiquitination of PKM2 and LDHA.

KEYWORDS
CTLH complex, glycolysis, LDHA, PKM, ubiquitination

Abbreviations: CTLH, C-terminal to LisH; diGLY, diglycine; ECAR, extracellular acidification rate; ENO1, alpha-enolase; Gid, glucose-induced degradation-deficient; GO, gene ontology; IP, immunoprecipitation; LC-MS/MS, liquid chromatography-tandem mass spectrometry; LDHA, L-lactate dehydrogenase A chain; LFQ, label-free quantification; LisH, lissencephaly type-1-like homology; MKLN1, muskelin; PEP, phosphoenolpyruvate; PKM, pyruvate kinase M1/2; PPP, pentose phosphate pathway; RanBPM, Ran-binding protein 9; RING, really interesting new gene domain; RMND5A, E3 ubiquitin-protein transferase required for meiotic nuclear division 5 homolog A; shControl, negative control short hairpin RNA; shRanBPM, short hairpin RNA directed against RanBPM.

1 | INTRODUCTION

Cells utilize multiple pathways to maintain metabolic flux. Glycolysis, an important example of this, is a series of enzymatic reactions in the cytosol that convert glucose into pyruvate, ATP, and NADH. In a key step of the glycolysis pathway, pyruvate kinase (PK) converts phosphoenolpyruvate (PEP) to pyruvate.[1] Pyruvate is then converted into either lactate by lactate dehydrogenase (LDH) or transported into the mitochondria and fed into the tricarboxylic acid (TCA) cycle. Intermediate metabolites of glycolysis can be used as precursors for anabolic pathways, such as the pentose phosphate pathway (PPP), glycogen synthesis, fatty acid synthesis, and amino acid synthesis.[2,3] High glycolytic flux is frequently observed in multiple cancer types and is believed to support growth of a rapidly proliferating cell by increasing cellular energetics and biosynthetic building blocks.[2-4]

In *Saccharomyces cerevisiae*, gluconeogenesis, which, in overall effect, is the reversal of glycolysis, is regulated in part by the glucose-induced degradation-deficient (Gid) complex.[5,6] The Gid complex is a multi-subunit really interesting new gene (RING) E3 ligase. RING E3 ligases confer substrate specificity in ubiquitination, the covalent attachment of ubiquitin molecules to lysine residues.[7-9] Ubiquitination can elicit a variety of effects, such as signaling for proteasomal degradation, changes in protein binding partners, enzymatic activity, and subcellular localization and its deregulation contributes to several disease phenotypes, in particular cancer.[10,11] Upon glucose replenishment in *S cerevisiae* cells that were deprived of glucose for 24 hours, the Gid complex facilitates polyubiquitination of the gluconeogenic enzymes fructose-1,6-bisphosphatase (Fbp1), isocitrate lyase (Icl1), malate dehydrogenase (Mdh2), and phosphoenolpyruvate carboxykinase (Pck1), leading to their proteasomal degradation and resulting in the inhibition of gluconeogenesis.[5,12,13] Ubiquitination of these enzymes by the Gid complex is triggered by the glucose-dependent induction and association of subunit Gid4, which recognizes the N-terminal prolines of the gluconeogenic enzymes.[5,6,12] Recently, cryo-EM structural determination of the Gid complex revealed that it exists in an anticipatory conformation that can switch to its active conformation upon Gid4 association, thus enabling rapid regulation of glucose metabolism in response to changing conditions.[6]

The Gid complex is evolutionarily conserved and its mammalian homologue is termed the C-terminal to LisH (CTLH) complex.[14,15] We and others have recently demonstrated that the mammalian CTLH complex exhibits E3 ligase activity in human cells and has at least nine subunits: RanBPM (Ran-binding protein M, aka RanBP9), TWA1 (glucose-induced degradation protein 8 homolog, aka GID8), ARMC8 (α and β isoforms; armadillo repeat-containing protein 8), GID4 (glucose-induced degradation protein 4 homolog), MKLN1 (muskelin), WDR26 (WD repeat-containing protein 26), and the RING domain proteins, which are required for its E3 ligase activity, RMND5A (E3 ubiquitin-protein transferase RMND5A) and MAEA (E3 ubiquitin-protein transferase MAEA).[15-17] A fascinating and conserved feature of the CTLH complex is the shared presence and order of appearance of lissencephaly type-1-like homology (LisH), CTLH, and CT11-RanBPM (CRA) α-helical domains present in RanBPM, TWA1, RMND5A, and MAEA, with muskelin and WDR26 also containing LisH and CTLH domains.[14,15] Additionally, discoidin and SPRY (named from SPla and the RYanodine Receptor) domains, and kelch, WD40, and armadillo (ARM) repeats comprise the variety of protein-protein interaction surfaces on CTLH complex subunits.

A functional understanding of the mammalian CTLH complex is still limited but recent work suggests its ubiquitination targets, or proteins it regulates, include HBP1 (HMG box-containing protein 1), LMNB2 (lamin B2), PRKAA (the catalytic subunit of AMP-activated protein kinase (AMPK)), c-Raf (RAF proto-oncogene serine/threonine-protein kinase, also called RAF1), HDAC6 (histone deacetylase 6), and its own subunit muskelin.[16-21] In the cancer context, individual subunits of the complex have been found to be either growth promoting or suppressive, which is likely dependent on cell type and contextual determinants.[20,22-24] Positive or negative regulation of several oncogenic pathways (eg, MAPK/ERK, WNT, TGFβ, NFκB, cell cycle) has been linked to individual subunit regulations, although, in almost all cases, whether the regulation involves the ubiquitin activity of the complex was not investigated.[13,22,23]

Here, we integrated three mass spectrometry-based proteomic techniques to uncover candidate ubiquitination targets and novel functions of the mammalian CTLH complex in HeLa cells. Using global and diglycine (diGLY)-enriched (ubiquitinome) label-free proteomics and affinity purification mass spectrometry using a RanBPM antibody, we identified several candidate ubiquitination targets, including three glycolytic enzymes. We show that the complex regulates ubiquitination and activity levels of pyruvate kinase M1/2 (PKM) and L-lactate dehydrogenase A chain (LDHA) glycolysis enzymes and functions to inhibit glycolytic flux and prevent altered metabolism. These results indicate that, like in yeast, the mammalian CTLH complex regulates glucose metabolism, albeit in a different manner, and reveal a multilevel post-translational negative regulation of glycolysis.

2 | MATERIALS AND METHODS

2.1 | Cell culture, plasmid construction, and antibodies

Wild-type, control short hairpin RNA (shRNA) stable (shControl), RanBPM shRNA stable (shRanBPM), CRISPR control and RMND5A KO HeLa cells have been

described previously.[16,20,24] All cells were cultured in high glucose Dulbecco's modified Eagle's medium (Wisent Bioproducts, St. Bruno, Quebec, Canada) supplemented with 10% FBS, 1% sodium pyruvate, and 1% L-glutamine at 37°C and 5% CO_2. Cells were treated with 10 μM MG132 (EMD-CalBiochem, San Diego, CA, USA) for 4 hours. Plasmid transfections were carried out with jetPRIME (Polypus Transfection, Illkirch, France) according to the manufacturer's protocol. pCDNA-FLAG-LDHA was created by PCR amplification (5′ GTACCAACCGGTA TGGCAACTCTAAAGGATC, 5′ GAAGGGTCTAGA TTAA ATTGCAGCTCCTTTTGGATCCC) of human LDHA cDNA (kind gift from Dr Rob Cumming) and cloned into pCDNA-FLAG (generated by digestion of muskelin of pCDNA-FLAG-MKLN1, described in Maitland et al[16]) via Age1 and XbaI digestion of both PCR product and vector. pCDNA-FLAG-PKM2 was created in the same way (5′ AATGCAC CGGTAGCAAGCCCCATAGTGAAGCC, 5′ AAAAAGGCTAGCCGG CACAGGAACAACACGC) using PKM2 human cDNA (kind gift from Dr John Di Guglielmo), but with the PCR product digested with Age1 and NHE1. Antibodies used for western blot were: ARMC8 (E-1, sc-365307; Santa Cruz Biotechnology, Santa Cruz, CA, USA), FLAG (M2, F1804, Sigma-Aldrich, St. Louis, MO, USA), HA (HA-7, H3663 Sigma-Aldrich), LDH (H-10, sc-133123, Santa Cruz), Muskelin (C-12, sc-398956, Santa Cruz Biotechnology), PKM (C-11, sc-365684, Santa Cruz), RanBPM (5 M, 71-001, Bioacademia, Japan), and Vinculin (E1E9V, Cell Signaling Technology, Danvers, MA, USA).

2.2 | MS sample preparation for global proteomics

HeLa cells at 75%-80% confluency were trypsinized and cells were collected by centrifugation, then washed in PBS and frozen at −80°C. Cells were lysed by resuspension in 8 M urea, 50 mM ammonium bicarbonate (ABC), 10 mM Dithiothreitol (DTT), 2% Sodium dodecyl sulfate (SDS) and then sonicated with a probe sonicator (Sonic Dismembrator, model 100; 20 × 0.5 s pulses, Level 1, Fisher Scientific, Hampton, NH, USA). Twenty-five microgram of protein lysate, as quantified by Pierce 660 nm Protein Assay (#22660, #22663, ThermoFisher Scientific, Waltham, MA, USA) was reduced in 10 mM DTT for 25 minutes, alkylated in 10 mM iodoacetamide for 25 minutes in the dark, followed by methanol precipitation as described in Kuljanin et al.[25] The protein pellet was resuspended in 50 mM ABC and subjected to a sequential digest first with 250 ng of LysC (125-05061, Wako Pure Chemical Ind., Ltd., Japan) for 4 hours, then 500 ng of Trypsin/LysC (V5071, Promega, Madison, WI, USA) for 16 hours, followed by 500 ng of Trypsin (V5111, Promega) for an additional 4 hours. Digestions were incubated at 37°C at 600 rpm with interval mixing (30 seconds mix, 2 minutes pause) on a Thermomixer C (cat# 2231000667, Eppendorf, Hamburg, Germany). After the last digestion, samples were acidified with 10% formic acid (FA) to pH 3-4 and centrifuged at 14 000 *g* to pellet insoluble material.

2.3 | diGLY enrichment

HeLa cells at 75%-80% confluency were treated with 10 μM MG132 for 4 hours and processed exactly as described for global proteomics. After methanol precipitation, 1 mg protein was digested sequentially as described for global proteomics but with 6.66 μg of Lys-C, 20 μg of Trypsin/Lys-C, and 20 μg of Trypsin. Peptides were then dried using a SpeedVac (Thermo Scientific). PTMScan Ubiquitin Remnant Motif (K-ε-GG, aka diGLY) Antibody Bead Conjugate (Cell Signaling Technology, #5562) (25 μL per sample) was cross-linked and used as described in Udeshi et al.[26] Briefly, antibody-bead conjugate was washed three times in 100 mM sodium borate, pH 9 (M5162, Sigma-Aldrich), then resuspended in 20 mM DMP (Dimethyl pimelimidate dihydrochloride, D8388, Sigma-Aldrich) in 100 mM sodium borate, pH 9 and rotated at room temperature for 30 minutes. Cross-linking was quenched by washing and incubation in 200 mM ethanolamine, pH 8 (S9640, Sigma-Aldrich) for 2 hours at 4°C with end-over-end rotation. After blocking, beads were washed three times with 1 mL of 1× IAP buffer (provided by the kit) and kept on ice. Dried peptides were resuspended in 1 mL of IAP buffer, centrifuged, and the supernatant was added to the cross-linked antibody beads and incubated with rotation for 1 hour at 4°C. After enrichment, beads were washed twice with IAP buffer, three times with PBS, and then peptides were eluted with two rounds of 5-minute incubations in 0.15% trifluoroacetic acid (TFA). The eluted peptides were dried in a SpeedVac and reconstituted in 0.1% FA.

2.4 | Liquid chromatography-tandem mass spectrometry (LC-MS/MS) for diGLY enrichment

Approximately 1 μg of peptide sample (as determined by Pierce BCA assay) was injected onto a Waters M-Class nanoAcquity UHPLC system (Waters, Milford, MA) coupled to an Orbitrap Elite mass spectrometer (ThermoFisher Scientific). Buffer A consisted of mass spectrometry grade water with 0.1% FA and buffer B consisted of acetonitrile with 0.1% FA (ThermoFisher Scientific). Samples were trapped for 4 minutes at a flow rate of 5 μL/min using 99% buffer A and 1% buffer B on an ACQUITY UPLC Symmetry BEH C18 Trapping Column (5 mm, 180 mm × 20 mm, Waters). Peptides were separated using an ACQUITY

UPLC Peptide BEH C18 Column (130 Å, 1.7 mm, 75 mm × 250 mm) operating at a flow rate of 300 nL/min at 35°C. Samples were separated using a non-linear gradient consisting of 1%-7.5% buffer B over 1 minute, 7.5%-25% buffer B over 179 minutes, 25%-32.5% buffer B over 40 minutes, and 32.5%-40% over 20 minutes, before increasing to 98% buffer B and washing. Full MS spectra were acquired in positive mode at R = 120 000 in the 400-1450 *m/z* mass range, 200 ms injection time, 1×10^6 ACG target. Top 20 peptides were selected for collision induced dissociation (ACG target: 1×10^5; injection time: 50 ms; min signal: 500; isolation width: 2.0 *m/z*; normalized collision energy: 35; activation time: 10 ms; charge exclusion: unassigned, 1; dynamic exclusion enabled 30 seconds).

2.5 | LC-MS/MS for global proteome

Approximately 1 µg of peptide sample (as determined by Pierce BCA assay) was injected onto a Waters M-Class nano-Acquity HPLC system (Waters) coupled to an ESI Orbitrap mass spectrometer (Q Exactive plus, ThermoFisher Scientific) operating in positive mode. Buffer A consisted of mass spectrometry grade water with 0.1% FA and buffer B consisted of acetonitrile with 0.1% FA (ThermoFisher Scientific). All samples were trapped for 5 minutes at a flow rate of 5 µL/min using 99% buffer A and 1% buffer B on a Symmetry BEH C18 Trapping Column (5 mm, 180 mm × 20 mm, Waters). Peptides were separated using a Peptide BEH C18 Column (130 Å, 1.7 mm, 75 mm × 250 mm) operating at a flow rate of 300 nL/min at 35°C (Waters). Proteome samples were separated using a non-linear gradient consisting of 1%-7% buffer B over 1 minute, 7%-23% buffer B over 179 minutes, and 23%-35% buffer B over 60 minutes, before increasing to 98% buffer B and washing. Full MS spectra were acquired in positive mode at R = 70 000 in the 400-1500 *m/z* mass range, 250 ms injection time, 3×10^6 ACG target. Top 12 peptides were selected for higher-energy collisional dissociation at R = 17 500 (ACG target: 2×10^5; injection time: 64 ms; loop count: 12; isolation width: 1.2 *m/z*; isolation offset: 0.5 *m/z*; normalized collision energy: 25; intensity threshold: 3.1×10^4; charge exclusion: unassigned, 1, 7, 8, >8; dynamic exclusion enabled 30 seconds).

2.6 | RanBPM affinity purification coupled to MS

Thirty micrograms of mouse IgG (sc-2025, Santa Cruz Biotechnology) or RanBPM (F-1, sc-271727, Santa Cruz Biotechnology) antibody was conjugated to 20 µL Dynabeads Protein G (10004D, Invitrogen, Life Technologies, Burlington, ON, Canada) for 1 hour at 4°C with end-over-end rotation. Afterwards, antibody-bead conjugate was cross-linked and quenched exactly as described above for the diGLY antibody. After quenching, cross-linked antibody and beads were then washed five times in lysis buffer and left on ice until ready. Meanwhile, HeLa WT cell pellets were lysed in whole-cell extract buffer (50 mM HEPES, pH7.4, 150 mM NaCl, 1 mM EDTA, 10% glycerol, 0.5% NP40, 1 mM DTT, 1 mM Na_3VO_4, 10 mM NaF, 1 mM phenylmethylsulfonyl fluoride (PMSF), 1 µg/mL of aprotinin, 10 µg/mL of pepstatin, and 1 µg/mL of leupeptin) for 25 minutes on ice and spun down at 13 000 rpm for 20 minutes at 4°C to pellet insoluble material. A volume corresponding to 1 mg of protein was adjusted to 0.25% NP40 and precleared with 3 µL Dynabeads Protein G for 30 minutes at 4°C with end-over-end rotation. Precleared extract was then added to the cross-linked antibody beads and incubated overnight at 4°C with end-over-end rotation. The next day, beads were washed and proteins eluted using a protocol adapted from Kaboord et al.[27] Briefly, beads were first washed three times with IP wash buffer (50 mM HEPES, pH7.4, 150 mM NaCl, 1 mM EDTA, 12% glycerol, 0.25% NP40), then three times in 50 mM ABC, followed by five times in HPLC grade water. Proteins were eluted with two rounds of 5-minute room temperature incubations in 0.5% FA, 30% acetonitrile with 1250 rpm shaking on a thermomixer. Pooled elutions were spun down briefly to collect any residual beads, transferred to a new tube and dried in a SpeedVac (Thermo Scientific). Dried protein was resuspended in 6 M urea and incubated in 10 mM DTT for 30 minutes, followed by 10 mM iodoacetamide for 25 minutes in the dark, and then methanol precipitated as described in Kuljanin et al.[25] Protein pellet was resuspended in 200 µL of 50 mM ABC and subjected to a sequential digest exactly as described for global proteomics. After the last digestion, samples were acidified with 10% FA to pH 3-4 and centrifuged at 14 000 *g* to pellet insoluble material. Supernatant was filtered by passing through a >10 kDa cellulose membrane (UFC501096, Sigma-Aldrich) and then was dried in a SpeedVac. Dried peptides were then resuspended in 0.1% TFA and desalted with C18 Ziptips (Z720070, Sigma-Aldrich). Eluted peptides were dried in a SpeedVac, resuspended in 20 µL 0.1% FA and 5 µL was injected onto a Waters M-Class nanoAcquity HPLC system (Waters) coupled to an ESI Orbitrap mass spectrometer (Q Exactive plus, ThermoFisher Scientific). Buffer A consisted of mass spectrometry grade water with 0.1% FA and buffer B consisted of acetonitrile with 0.1% FA (ThermoFisher Scientific). All samples were trapped for 5 minutes at a flow rate of 5 µL/min using 99% buffer A and 1% buffer B on a Symmetry BEH C18 Trapping Column (5 mm, 180 mm × 20 mm, Waters). Peptides were separated using a Peptide BEH C18 Column (130 Å, 1.7 mm, 75 mm × 250 mm) operating at a flow rate of 300 nL/min at 35°C (Waters). Samples were separated using a non-linear gradient consisting of 1%-7% buffer B over 1 minute, 7%-23% buffer B over 59 minutes, and 23%-35% buffer B over 20 minutes,

before increasing to 98% buffer B and washing. MS acquisition settings were the same as described for the proteome samples.

2.7 | Proteomic data analysis

All MS raw files were searched in MaxQuant version 1.5.8.3 using the Human Uniprot database (reviewed only; updated May 2017 with 42,183 entries).[28,29] Missed cleavages were set to 3, cysteine carbamidomethylation (CAM) was set as a fixed modification and oxidation (M), N-terminal acetylation (protein) and deamidation (NQ) (and for diGLY enrichment, GlyGly modification of lysine) were set as variable modifications (max. number of modifications per peptide = 5), and peptide length ≥6. Protein and peptide FDR was left to 0.01 (1%) and decoy database was set to revert. Match between runs was enabled and all other parameters left at default. Protein groups or GlyGly sites were loaded into Perseus (version 1.6.0.7) and proteins containing peptides only identified by site or matched to reverse and contaminant database were removed. diGLY sites were kept only if there was a localization score >0.9. After log2 transformation, protein groups or diGLY sites were only retained if they had valid values in ≥4 samples (out of 5) in either control or knockdown for proteome, ≥3 (out of 4) samples in RanBPM interactome, or ≥3 (out of 3) for diGLY. For proteome and diGLY analysis, peptide or protein group label-free quantification (LFQ) log2 transformed intensities were normalized to the median in each sample. In all datasets, missing values were imputed using a width of 0.3 and down shift of 1.8, and two-sided student's t tests were performed in Perseus. All data showed a normal distribution. Gene ontology (GO) and pathway analysis was performed using g:profiler.[30] Significantly increased or decreased protein lists were scored against the list of all quantified proteins in the particular dataset as the statistical domain scope, except for the interactome, which was set to "only annotated genes." Benjamini-Hochberg FDR was set to a significance threshold of 0.05 and "No electronic GO annotations" was enabled. Gene IDs were converted using g:Convert. Data sources selected: GO biological process, cellular compartment, and molecular function (2020-12-08); Reactome (2020-12-15); Wikipathways (2020-12-10); miRTarBase (Release 7.0); CORUM (03.09.2018 Corum 3.0); and Human Phenotype (hpo.annotations #1275). Only significantly enriched terms with a minimum size of 5 and maximum size of 350 were retained. Significant categories were then grouped based on similarity coefficient and visualized using EnrichmentMap (version 3.3.1)[31] and AutoAnnotate (version 1.3.3)[32] applications in Cytoscape (version 3.8.0)[33] following the protocol in Reimand et al.[34] For the RanBPM associated proteins, an interactor was considered if $P < .05$ and >2.0 fold enriched in RanBPM IP vs IgG negative control. The RanBPM interactome map was made using Cytoscape and edges were determined by STRING database (confidence score >0.4).

2.8 | In vivo ubiquitination for Western blot

To validate ubiquitination of LDHA and PKM2, cells were transfected with pCDNA-FLAG-LDHA or pCDNA-FLAG-PKM2 and/or pMT123 plasmid expressing HA-ubiquitin. Twenty hours after transfection, cells were treated with 10 μM MG132 for 4 hours then collected, pelleted, and frozen. Cells were lysed in freshly made Buffer A (50 mM Tris, pH 7.5, 150 mM NaCl, 1% Triton, 1% SDS, 1 mM Na_3VO_4, 10 mM NaF, 1 mM PMSF, 1 μg/mL of aprotinin, 10 μg/mL of peptatin, 1 μg/mL of leupeptin, and 25 mM NEM (N-Ethylmaleimide, Bioshop Canada, Burlington, ON, Canada)), sonicated with a probe sonicator (Fisher Scientific Sonic Dismembrator, model 100; 30 × 1 second pulses at power level 2) and incubated on ice for 30 minutes, and then insoluble material pelleted by centrifugation. Lysates were quantified using 660 nm protein assay (Thermo, #22660, #22663). For immunoprecipitation, lysates (500 μg) were diluted 1:10 in buffer B (buffer A with no SDS) and incubated with 3 μL of anti-FLAG (M2; F1804; Sigma-Aldrich) overnight at 4°C, followed by incubation with Dynabeads Protein G (10004D, Invitrogen) for 1 hour. Beads were washed five times in buffer B then resuspended and boiled at 95°C in SDS loading dye. Samples were run on a 10% SDS-polyacrylamide gel electrophoresis (SDS-PAGE) for LDHA and 8% SDS-PAGE for PKM2 and gels were transferred to polyvinylidene fluoride membrane and blocked in 5% milk.

2.9 | Central carbon metabolism profiling

Exponentially growing shControl or shRanBPM cells were pelleted by brief centrifugation then snap frozen in dry ice/ethanol bath and stored at −80°C. Samples were processed as a service for quantitation of Central Carbon Metabolism metabolites in cell pellets by UPLC-MRM/MS at the University of Victoria Genome BC Proteomics Centre and The Metabolomics Innovation Centre.

2.10 | PK and LDH activity assays

Colorimetric Pyruvate Kinase Activity Assay Kit (Sigma-Aldrich, MAK072) and Lactate Dehydrogenase Activity Assay Kit (Sigma-Aldrich, MAK066) were used according to the manufacturer's instructions. Briefly, $1x10^6$ cells were collected, washed in PBS, snap frozen, and stored at −80°C. Cells were lysed in 250 μL of the assay buffer and

centrifuged. The supernatant was diluted 1:100 and 50 μL of it was used for the assay. Activity was determined as the difference in absorbance (450 nm for LDH, 570 nm for PKM) between the penultimate reading before saturation and $T_{initial}$, then compared to standard curve and calculated as nmole/min/mL. Activity was normalized to protein concentration in extracts as calculated by BCA assay.

2.11 | Measurement of glycolysis in real time

Glycolysis was measured using Agilent Seahorse XF Glycolysis Stress Test and Extracellular Acidification Rate (ECAR) with a XFe24 Seahorse analyzer (Agilent Technologies, Santa Clara, CA, USA) according to the manufacturer's instructions. Briefly, shControl and shRanBPM HeLa cells were seeded onto XFe24 Seahorse plates at 2.5×10^4 cells per well. Culture media were exchanged for unbuffered media supplemented with 2 mM glutamine 1 hour before the assay. After basal metabolic readings were recorded, substrates and selective inhibitors were injected to achieve final concentrations of glucose (10 mM), oligomycin (1 μM), and 2-deoxyglucose, (2-DG, 50 mM). Changes in oxygen consumption rate (OCR) and ECAR in response to the addition of substrates/inhibitors were described as the mean change after injection compared with the average OCR or ECAR before the injection. The OCR and ECAR values were normalized to protein concentration from each well.

2.12 | Statistical analysis

Non-proteomic data statistical analyses were performed using GraphPad PRISM (version 9.0.1). Differences between two groups were compared using unpaired two-tailed Student's t test. Results were considered significant when $P < .05$. Biological replicate numbers are indicated in figure legend and exact P or q values are indicated in the text.

3 | RESULTS

RanBPM was previously shown to be essential for CTLH complex stability.[16] To comprehensively identify candidate ubiquitination substrates of the CTLH complex, we used global and diGLY-enriched mass spectrometry-based quantitative proteomics in RanBPM knockdown cells in conjunction with the identification of associated proteins of the endogenous complex by affinity purification mass spectrometry. The goal was to compare these different screens to confidently identify ubiquitination targets of the complex. For example, a protein that shows an association in the interactome with a RanBPM-dependent increase in protein abundance and/or decrease in ubiquitination would represent a candidate ubiquitination target of the complex.

3.1 | RanBPM-dependent global proteome

First, we assessed RanBPM-dependent changes in protein abundance by comparing the global proteomes of shControl and shRanBPM HeLa cells (Figures 1A and S1). After filtering, a total of 4835 proteins were used for downstream analysis (Supplemental File S1). Sixty-one proteins were significantly increased ($P < .05$, fold change >2.0) and 38 were significantly decreased ($P < .05$, fold change <−2.0) in shRanBPM cells compared to the shControl cells (Figure 1B). This included RanBPM itself and previously reported protein level changes, such as a decrease in TWA1/GID8.[16] We analyzed the list of RanBPM-dependent increased and decreased proteins for statistical enrichment using g:profiler with Benjamini-Hochberg FDR correction of gene ontology (GO) terms and pathways. Proteins related to lipoprotein particle binding ($q = 0.007$), axon ($q = 0.0006$) and dendrite ($q = 0.035$), amino acid binding ($q = 0.028$), and dopamine receptor binding ($q = 0.0086$), among others, were enriched among the increased proteins (Figure 1C, top). For decreased proteins, terms enriched included molecular transducer activity ($q = 0.011$), signaling receptor activity ($q = 0.011$), inflammatory response pathway ($q = 0.019$), and cardiac progenitor differentiation ($q = 0.001$) (Figure 1C, bottom).

We compared the changes at the proteome level to a previously conducted microarray analysis which was also done using the same shRanBPM HeLa cells (Figure 1D, Supplemental File S2).[35] Proteome vs RNA changes showed a relatively modest correlation ($R^2 = 0.301$, $P < .0001$) (Figure 1D). The candidates that showed the greatest changes (either increasing or decreasing) at the protein level, however, also showed large differences at the RNA level (eg, THY1 (Thy-1 membrane glycoprotein), ALPL (alkaline phosphatase, tissue-nonspecific isozyme), BCAT1 (branched-chain amino acid aminotransferase, cytosolic), OAS3 (2′-5′-oligoadenylate synthase 3), and CRYAB (alpha-crystallin B chain)), indicating that the levels of these proteins were changed due to transcriptional effects rather than post-translational regulations (Figure 1D). Therefore, we made note of several proteins that were found significantly increased in the proteome but not at the RNA level in shRanBPM cells since some of these may be regulated by ubiquitination resulting in degradation. LRP8 (low-density lipoprotein receptor-related protein 8), PPP1R9B (neurabin-2), AP4E1 (AP-4 complex subunit epsilon-1), KCNK1 (potassium channel subfamily K member 1), ANKRD52 (serine/threonine-protein phosphatase 6 regulatory ankyrin repeat subunit C), and CYFIP2 (cytoplasmic FMR1-interacting protein 2) were proteins with a large significant protein fold change, but a minimal change in RNA levels (Figure 1D).

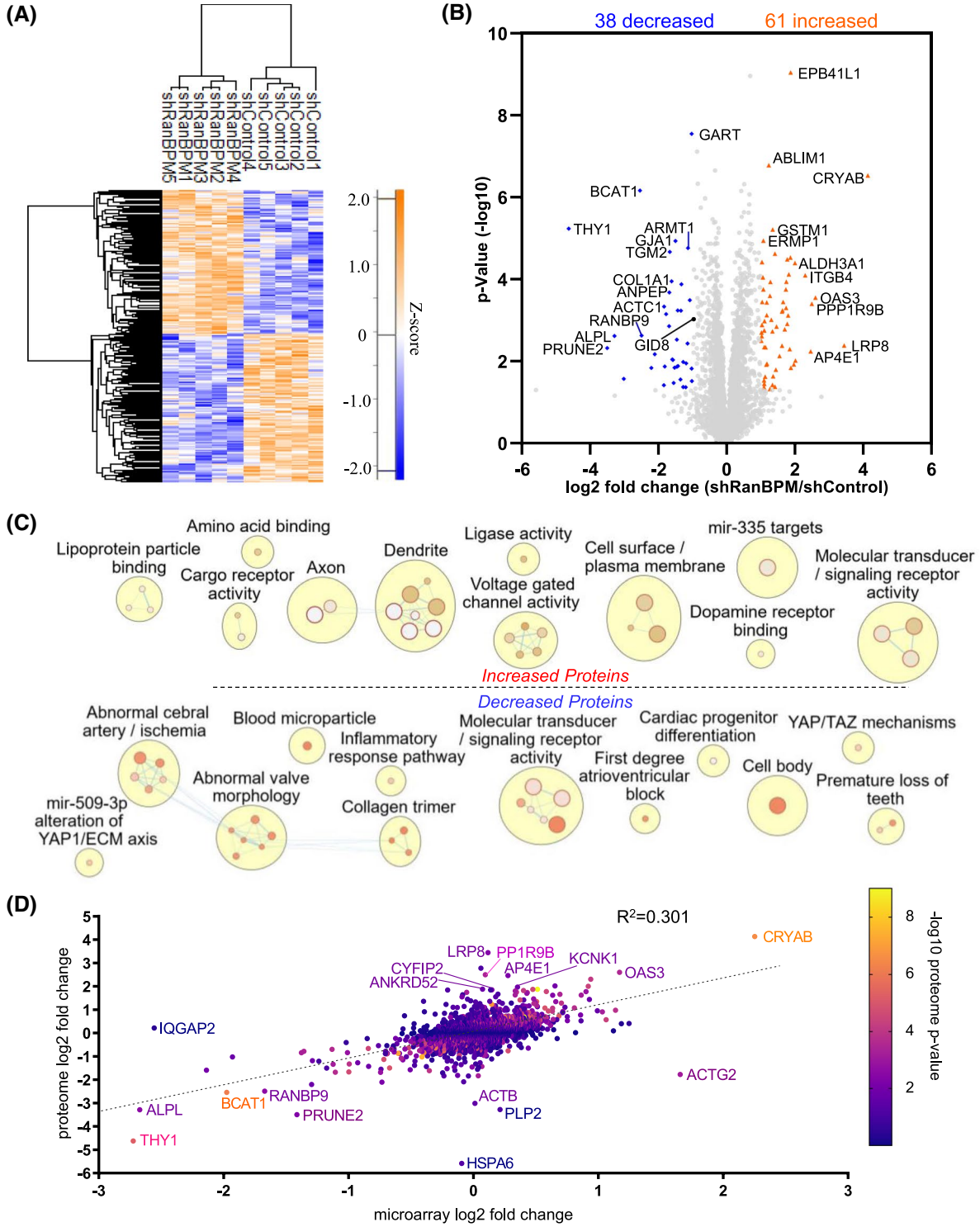

FIGURE 1 The RanBPM-dependent HeLa proteome. A, Heatmap clustering representation across samples of significantly changed proteins ($P < .05$). B, Volcano plot showing distribution of log2 fold change and –log10 P-value of all quantified proteins, n = 5. Blue diamonds: $P < .05$, fold change <−2; orange triangles: $P < .05$, fold change >2. Proteins with separation in the plot or noted in the text are labeled with their gene name. C, GO terms and pathways significantly enriched (q-value < 0.05, Benjamini-Hochberg FDR) in either increased proteins (top) or decreased proteins (bottom). Terms (nodes) were clustered and grouped (yellow circles) based on their similarity coefficient. Size of the node reflects size of the term, and color reflects q-value ranging from orange (0.05) to white (0). D, Comparison of shRanBPM proteome vs previous microarray data. Proteins quantified in the RanBPM-dependent proteome were matched with their RNA change in Atabakhsh et al, 2012. Dots are colored according to the corresponding −log10 P-value in the proteome

3.2 | RanBPM-dependent ubiquitinome

Next, we assessed the RanBPM-dependent ubiquitinome by enriching for the diGLY remnant, which is present on lysines in tryptic peptides originating from ubiquitinated proteins.[26] Extracts prepared from shControl and shRanBPM HeLa cells treated with MG132 were subjected to LysC/trypsin digestion and diGLY peptides were enriched using a specific antibody. Using label-free quantification, we quantified a total of 13 429 ubiquitin sites, with 5232 used for downstream analysis after filtering (Figure S2, Supplemental File S3). We found 205 ubiquitin sites significantly decreased in shRanBPM cells ($P < .05$, fold change <-2), and 129 significantly increased ($P < .05$, fold change >2) (Figure S2).

We compared the significant ($P < .05$) ubiquitin changes to the corresponding total protein change from the proteome analysis (Figure 2A). Here, any ubiquitin sites that changed in the same direction as its corresponding protein in the shRanBPM-dependent proteome more than 1.5-fold (black circles in Figure 2A), or were not detected in the proteome, were omitted from further analysis. This was done so that changing total protein levels would not confound differences in ubiquitination. Using a diGLY enrichment fold change cutoff at 1.5, 88 increased and 234 decreased ubiquitin sites were remaining. Surprisingly, no proteins that increased more than 1.5-fold at the protein level had at least a 1.5-fold decreased ubiquitin site (Figure 2A). GJA1 (gap junction protein alpha 1) and SOAT1 (sterol o-acyltransferase 1) were decreased at least 1.5-fold at the protein level and had an increased ubiquitination site (Figure 2A). All others were not changed at the protein level. For RanBPM-dependent increased ubiquitinated proteins, terms such as hemostasis ($q = 0.016$), plasma membrane region ($q = 0.028$) and protein complex involved in cell adhesion ($q = 0.028$) were enriched (Figure 2B, top). ATPase activity ($q = 0.014$), small molecule metabolic process ($q = 0.02$), RNA localization ($q = 0.015$), mitochondrial matrix ($q = 0.028$), and translation regulator activity ($q = 0.02$) were enriched within proteins with RanBPM-dependent decreased ubiquitination (Figure 2B, bottom).

3.3 | The endogenous RanBPM interactome

To narrow down our list of candidate ubiquitin substrates to those that associate with the complex, we identified CTLH complex associated proteins using a specific RanBPM antibody and affinity purification mass spectrometry. Besides the 9 CTLH members, 85 other associated proteins were

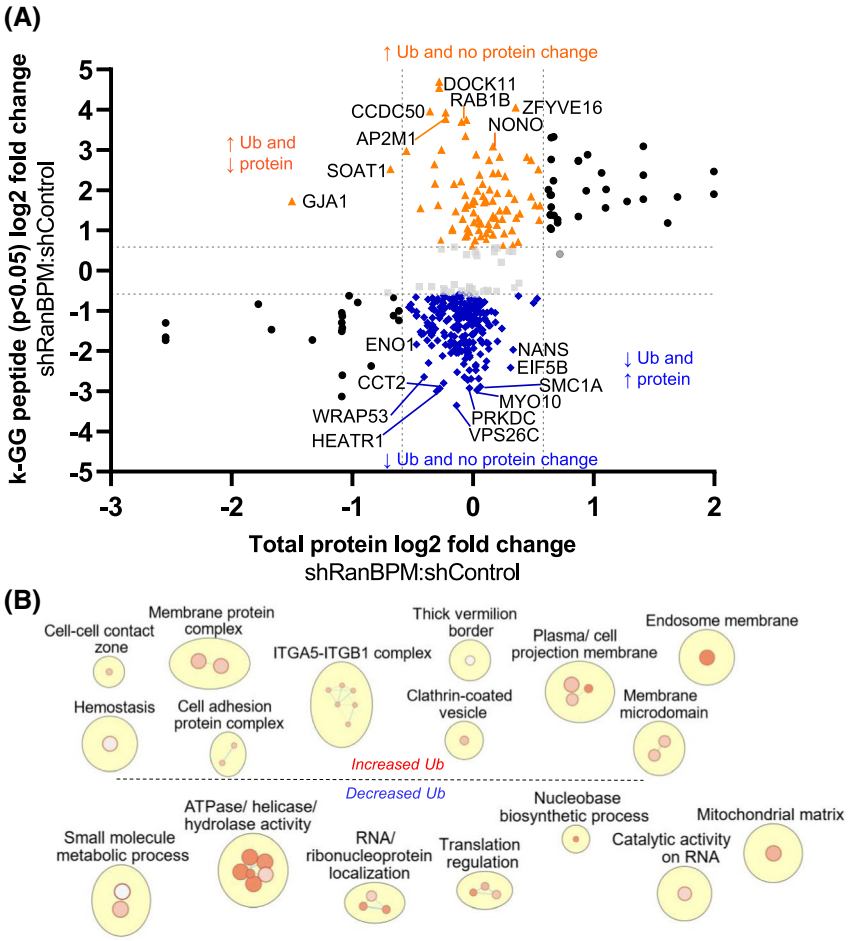

FIGURE 2 The RanBPM-dependent HeLa ubiquitinome. A, Proteins with a significant diGLY site ($P < .05$) are plotted with their log2 fold change against the log2 fold change of their matched total protein levels from the proteome. Blue dots: diGLY fold change <-1.5, proteome fold change >-1.5; orange dots: diGLY fold change >1.5, proteome fold change <1.5. Proteins with separation in the plot or noted in the text are labeled with their gene name. B, GO terms and pathways significantly enriched (q-value < 0.05, Benjamini-Hochberg FDR) in proteins with either increased diGLY enrichment (top, orange triangles in A) or decreased diGLY enrichment (bottom, blue diamonds in A). Terms (nodes) were clustered and grouped (yellow circles) based on their similarity coefficient. Size of the node reflects size of the term, and color reflects q-value ranging from orange (0.05) to white (0)

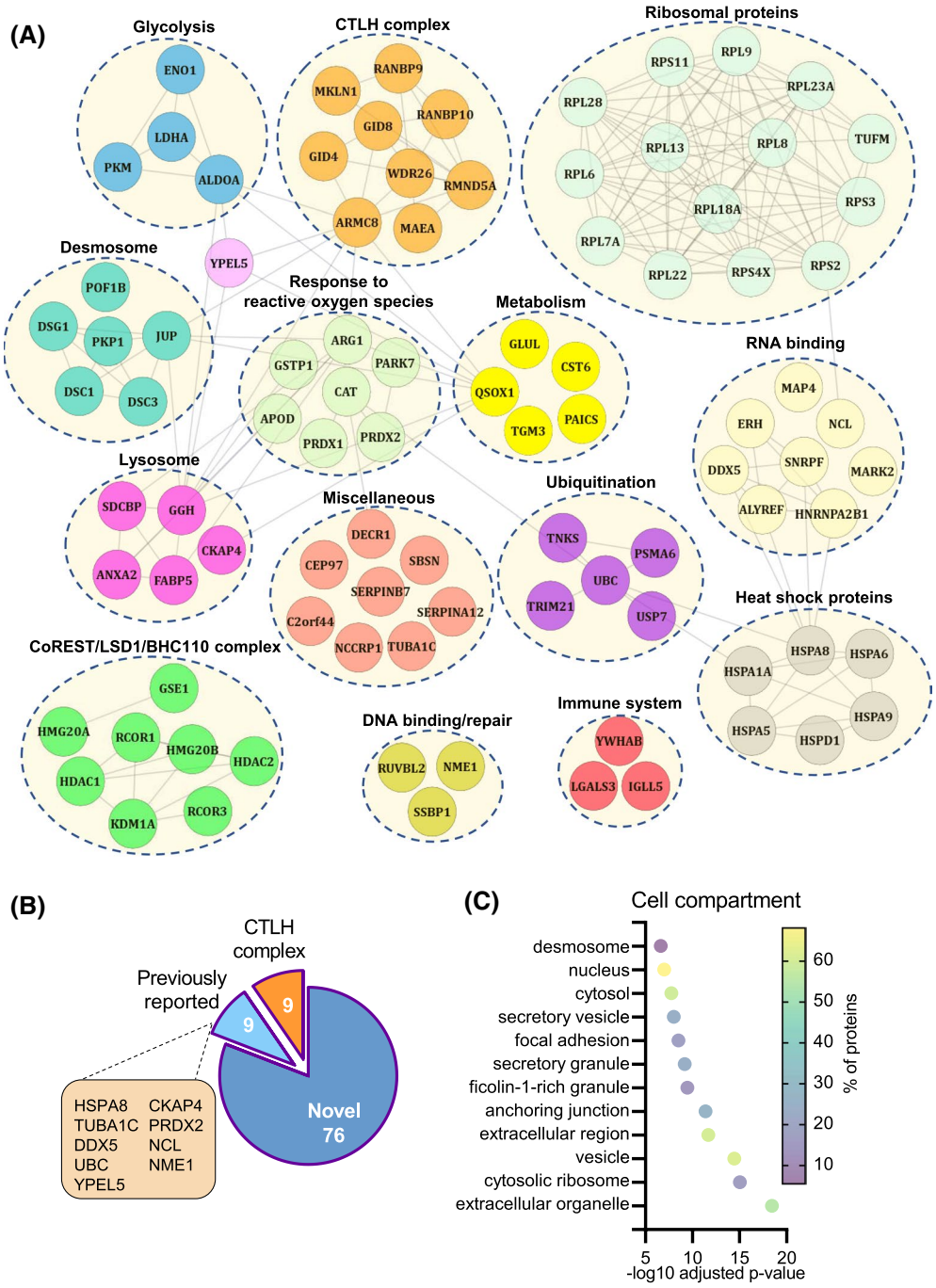

FIGURE 3 The endogenous RanBPM interactome in HeLa cells. A, Mass spectrometry identified proteins in anti-RanBPM immunoprecipitations in HeLa cells clustered based on STRING interaction and biological theme. B, Distribution of identified associated proteins as novel or as previously reported. C, Distribution of non-redundant top 12 significantly (q-value < .05, Benjamini-Hochberg FDR) enriched GO cell compartments

identified, including 9 previously reported to associate with subunits of the CTLH complex and 76 novel interactors (Figure 3A,B, Supplemental File S4).[17,23,36-39] Among those CTLH-associated proteins were the coREST transcriptional repressor complex, ribosomal proteins, heat shock chaperones, lysosomal proteins, RNA binding proteins, proteins associated with desmosomes, and glycolysis enzymes (Figure 3A). GO cellular compartment analysis revealed that the associated proteins were near equally associated with the cytoplasm and nucleus, consistent with the complex being present in both compartments,[15,16] with enrichment as well in extracellular organelles, focal adhesion, and vesicles (Figure 3C).

GLUL (glutamine synthetase) was the only protein increased in abundance in the proteome that was identified in the RanBPM interactome (Figure 4A). Comparison of the

RanBPM interactome to the list of decreased diGLY sites revealed six proteins in common which are likely to be non-degradative ubiquitin targets of the complex: ENO1 (alpha-enolase), HSPD1 (60 kDa heat shock protein, mitochondrial), LDHA (lactate Dehydrogenase A), PAICS (multifunctional protein ADE2), RPS25 (ribosomal protein S25), and PKM (pyruvate kinase) (Figure 4A). Interestingly, three of these proteins (PKM, LDHA, and ENO1) are key enzymes involved in the glycolysis pathway (Figure 4B).

3.4 | Polyubiquitination of PKM2 and LDHA is regulated by the CTLH complex

We focused on the glycolytic enzymes, intrigued by the connection of the yeast complex with glucose regulation.[5] We validated PKM2 and LDHA as interactors of the complex by immunoprecipitating FLAG-tagged construct of each enzyme and looking for the co-IP of CTLH subunits (Figure 5A,B). Additionally, we observed reduced polyubiquitination of transfected PKM2 and LDHA in an IP under denaturing conditions in both shRanBPM and RMND5A KO HeLa cells compared to their respective control cell lines (Figure 5C-F). These results confirmed the data from the diGLY and RanBPM interactome mass spectrometry analysis and indicate that the CTLH complex associates with and regulates polyubiquitination of LDHA and PKM2.

3.5 | Glycolysis is enhanced and metabolism is altered in shRanBPM cells

The global proteome data indicated that protein levels of PKM2 and LDHA were not changed in shRanBPM HeLa cells. We confirmed this by western blot using antibodies

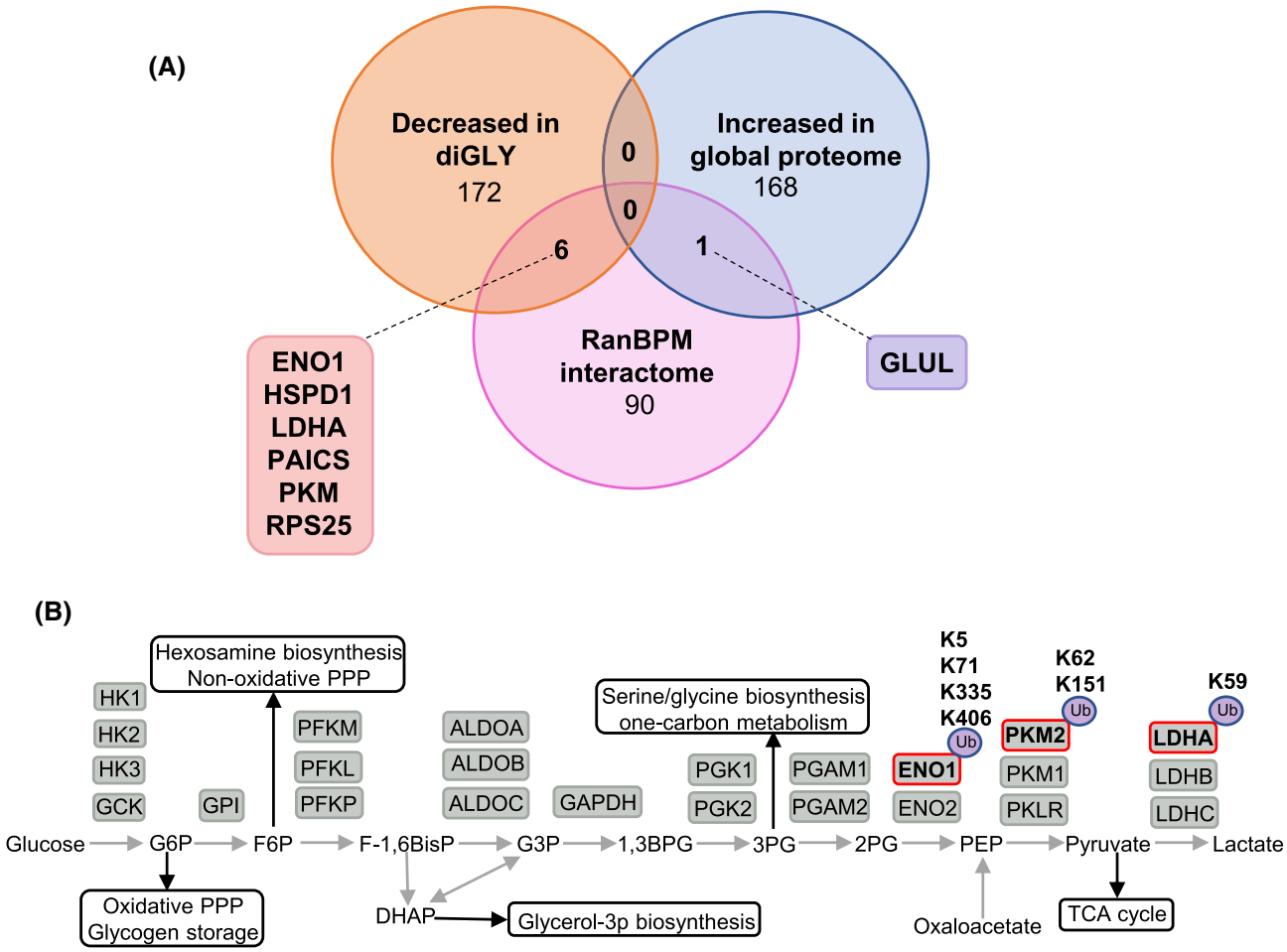

FIGURE 4 Comparisons of the RanBPM interactome with increased proteins and decreased ubiquitination. A, Comparison of the RanBPM associated proteins to the proteins increased (>1.5-fold, $P < .05$) in the proteome dataset and to the proteins with a decreased ubiquitin site (<−1.5-fold, $P < .05$ in diGLY dataset but >−1.5-fold changed at proteome) in shRanBPM cells. B, Glycolysis pathway with proteins containing reduced diGLY sites in shRanBPM cells circled in red and indicated with Ub. The lysine residue(s) with decreased ubiquitination are indicated. G6P: glucose-6-P; PPP: pentose phosphate pathway; F6P: fructose-6-P; F-1,6-BisP: fructose-1,6-PP; DHAP: dihydroxyacetone-P G3P: glyceraldehyde-3-P; 1,3BPG: 1,3-PP-glycerate; 3PG; 3-P-glycerate; 2PG: 2-P-glycerate; PEP: phosphoenolpyruvate; TCA: tricarboxylic acid

directed against LDH and PKM (Figure 6A). Thus, the CTLH complex-dependent ubiquitination of PKM and LDHA likely affects these enzymes in ways other than degradation. Since PTM regulation (including ubiquitination) has previously been reported to induce changes in LDH and PKM catalytic activity,[40,41] we assessed PK and LDH activities in extracts of shRanBPM HeLa cells. Activity assays showed significantly increased activity of both PK (1.47-fold, $P = .036$) and LDH (1.42-fold, $P = .0058$) in shRanBPM cells (Figure 6B). These findings indicate that ubiquitination of PKM and LDHA mediated by the CTLH complex functions to inhibit activity of both proteins.

To determine if the regulation of PKM2 and LDHA by the CTLH complex impacts glycolysis, we measured glycolysis in real time using a Seahorse extra cellular acidification rate (ECAR) assay. Glycolysis (1.44-fold, $P = .036$), glycolytic capacity (1.67-fold, $P = .025$), and glycolytic reserve (1.73-fold, $P = .01$) were all significantly higher in shRanBPM HeLa cells compared to shControl cells, suggesting that the CTLH complex functions to inhibit glycolysis in this cell type

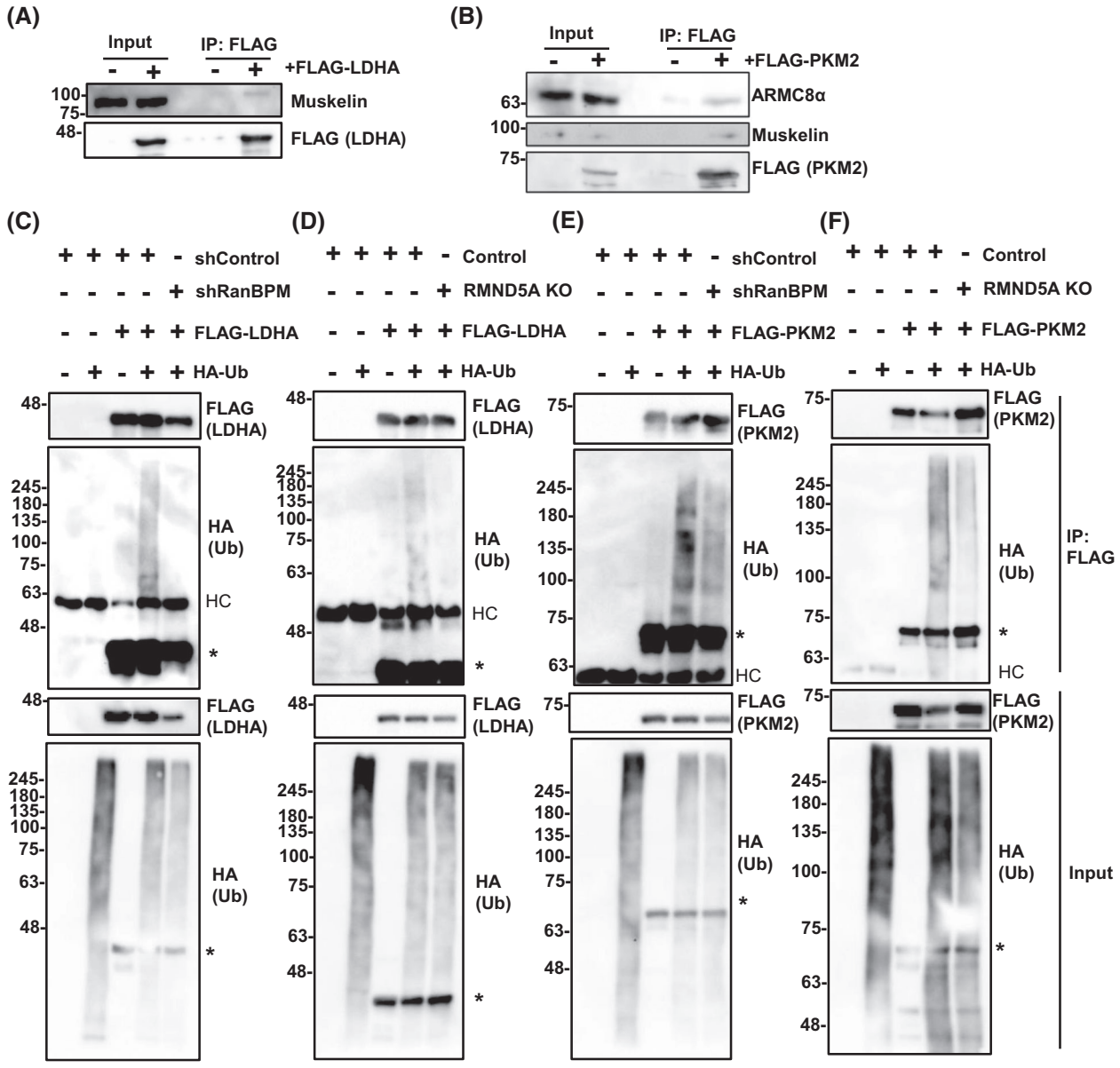

FIGURE 5 CTLH complex-dependent ubiquitination of glycolysis enzymes. A and B, LDHA and PKM associate with CTLH complex subunits. Transfected FLAG-LDHA (A) or FLAG-PKM2 (B) in WT HeLa cells were immunoprecipitated (IP) with FLAG antibody and analyzed by Western blot with antibodies against FLAG and the indicated CTLH complex subunits. Representative gel shown from n = 3 biological replicates. C-F, Reduced polyubiquitination of LDHA and PKM2 in shRanBPM and RMND5A KO HeLa cells. Transfected FLAG-LDHA or FLAG-PKM2 co-transfected with HA-ubiquitin in the indicated cell lines treated with MG132 were lysed in denaturing conditions and subjected to IP with FLAG antibody. * indicates previous FLAG hybridization. HC: heavy chain of IP antibody. Representative gel shown from n = 3 biological replicates

(Figure 6C). This was further supported by targeted mass spectrometry-based quantification of intracellular central carbon metabolites, which revealed most of the glycolytic intermediates, such as glucose-6-phosphate, fructose-6-phosphate, mannose-6-phosphate, glycerate-1,3-bisphosphate, PEP, and pyruvate, were increased in shRanBPM HeLa cells compared to shControl cells (Figure 6D). Additionally, metabolites of other pathways were affected, as RanBPM shRNA cells had increased glucosamine-6P, erythrose-4p, and phosphocreatine, and decreased glycerol-3 phosphate and ribose. Surprisingly, little changes were observed in TCA metabolites, although α-ketoglutaric acid was increased. Among nucleotides, ATP (1.22-fold, $P = .041$), GTP (1.35-fold, $P = .034$), and ATP/ADP ratio (1.52-fold, $P = .013$) were significantly increased in shRanBPM cells, while ADP (1.22-fold, $P = .002$), AMP (1.47-fold, $P = .01$), GMP (1.38-fold, $P = .023$), and NADPH (1.38-fold, $P = .022$) were significantly decreased (Figure 6E). Taken together, we conclude that the CTLH complex functions to negatively regulate glycolysis in HeLa cells.

4 | DISCUSSION

The human CTLH complex, homologue of the yeast Gid E3 ligase complex,[5,14] was recently demonstrated to have ubiquitin ligase activity.[16,17] Since then, a few of its substrates have been identified, including the transcription factor HBP1, nuclear matrix protein lamin B, and its own subunit muskelin.[16-18] In this report, we conducted a variety of high-throughput proteomic techniques that revealed candidate ubiquitination targets and insight into functions of the CTLH complex.

Several glycolysis enzymes emerged from the proteomic data as primary candidate targets for ubiquitination by the complex and further analyses revealed that glycolysis is deregulated in HeLa cells deficient in RanBPM, an essential CTLH complex member.[16] Our data suggest that the CTLH complex functions to normally restrict glycolytic flux at least in part by inhibiting the activity levels of PKM2 and LDHA, and potentially also ENO1, via ubiquitination. In the *S cerevisiae* complex, Gid4 binds N-terminal proline residues on gluconeogenic enzymes via its β-barrel domain.[12,42] Human GID4 also binds N-terminal proline peptides or other non-proline hydrophobic N-terminal peptides.[42,43] While formally unknown at this time, it is unlikely that the ubiquitination of the glycolysis enzymes by the CTLH complex involves GID4 since PKM2 and LDHA do not fit the GID4 binding criteria. Other confirmed or predicted ubiquitination targets of the human complex identified so far (HBP1, Lamin B2, AMPK, and c-Raf) also do not fit the hydrophobic N-terminal criteria.[17-20] This implies that the human complex has evolved beyond Gid4 binding of N-terminal proline proteins. The inclusion of muskelin in the vertebrate CTLH complexes is likely to be an important factor differentiating the human complex ubiquitin activity from the yeast complex.[14]

As part of the catabolite inactivation process in *S cerevisiae*, the Gid complex ubiquitinates Fbp1 and other gluconeogenic enzymes, resulting in their proteasomal degradation.[5,12] Regulation of gluconeogenesis and ubiquitination of gluconeogenic enzymes was previously ruled out for the human complex.[17] This is further supported by the findings of the current report that together suggest the mammalian complex evolved to regulate the opposing glucose regulation pathway. In doing so, it achieves the same overall function: maintenance of glucose metabolism homeostasis. Over evolutionary time, this change in mechanism may have been necessary due to differences in the gluconeogenic enzymes (eg, human Fbp1 does not have the N-terminal proline) and/or a shift in gluconeogenesis reliance (eg, in mammals, gluconeogenesis is primarily limited to the liver and kidney).

Glycolysis enzymes are regulated at the transcriptional level by proteins frequently altered in cancer (eg, HIF1, c-MYC, p53).[44] Post-translational modifications are also reported to regulate glycolysis enzymes, either by affecting protein stability, subcellular localization, or enzyme activity. For example, high glucose-stimulated acetylation of PKM2 inhibits its kinase activity and promotes its degradation by chaperone-mediated autophagy degradation,[45] while monoubiquitination of PKM2 by Parkin decreases PKM activity.[41] Phosphorylation of LDHA enhances its activity and is required to sustain high glycolytic flux[40] and nuclear translocation of GAPDH is regulated by PCAF-mediated acetylation.[46] Multiple glycolysis enzymes are targeted by p300 for lysine 2-hydroxyisobutyrylation (Khib), which enhances their activities.[47] Our findings uncover a second post-translation modifier that acts at multiple points within the glycolysis pathway, but one that inhibits activities. This ability of multiple glycolytic enzymes to be activated by p300-mediated Khib or inhibited by CTLH complex-mediated ubiquitination likely provides in a healthy cell the opportunity to coordinate and robustly control the amplitude of the glycolysis pathway in response to various stressors.

Our proteomic data and the findings of the effects of the CTLH complex on glycolysis add to the understanding of this complex and provide a novel function in carbon metabolism. Individual subunits have been linked with various signaling pathways, processes, and diseases, such as the WNT pathway, MAPK signaling, differentiation, development, cancer, and neurodegenerative diseases.[13,20,22,23,48-52] The CTLH complex as a unit has been functionally linked with nuclear condensation in developing erythroblasts through ubiquitination of at least lamin B.[18] It has also been determined to ubiquitinate HBP1 to promote cell proliferation.[17] In both cases, CTLH complex-dependent ubiquitination regulates proteasomal degradation and involves in vitro assays that used UBE2H (ubiquitin-conjugating enzyme E2 H) as the E2 enzyme. The

CTLH regulation of three other predicted targets, muskelin, c-Raf, and AMPK, also involve their proteasomal degradation.[16,19,20] The drosophila CTLH complex with the UBE2H homologue (named Kdo) is responsible for timed proteasomal degradation of an essential RNA binding complex during the maternal to zygotic transition.[53,54] This is also consistent with the yeast Gid complex ubiquitination of gluconeogenic enzymes, which results in their proteasomal degradation.[5] Thus, our findings provide the first evidence that CTLH complex ubiquitination affects a protein other than through

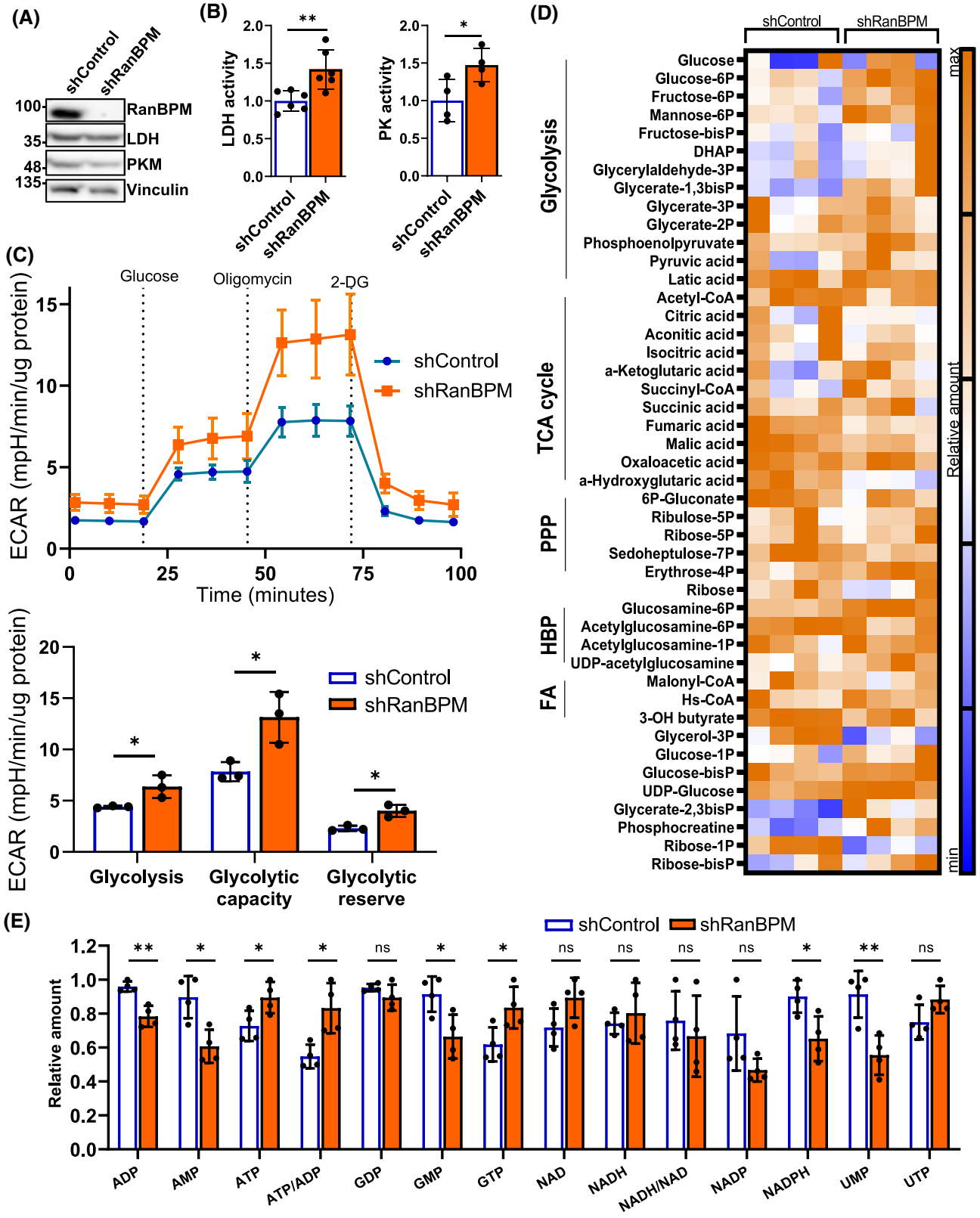

FIGURE 6 The CTLH complex regulates glycolysis. A, Western blot showing levels of LDH and PKM in shControl and shRanBPM HeLa cells. Representative gel shown from n = 3 biological replicates. B, Activities of LDH (left; n = 6) and PK (right; n = 4) in extracts of shControl and shRanBPM HeLa cells. Values were made relative to the mean of the control. Data are presented as mean ± SD. *$P < .05$, **$P < .01$ (Student's t test). C, *Top*, Extracellular acidification rate (ECAR) measuring during glycolysis stress test for shControl or shRanBPM HeLa cells. *Bottom*, ECAR measurements for glycolysis (after glucose injection), glycolytic capacity (maximum ECAR after oligomycin injection), and glycolytic reserve (after 2-Deoxy-d-glucose [2-DG] injection), n = 3. Data are presented as mean ± SD. *$P < .05$ (Student's t test). D, Heatmap representation of central carbon metabolites as measured by mass spectrometry. For each metabolite, values are relative to the highest value of the metabolite across the different samples set to 1 (dark orange). DHAP: dihydroxyacetone phosphate; PPP: pentose phosphate pathway; HBP: hexosamine biosynthetic pathway; FA: fatty acid. E, Relative amounts of nucleotides in shControl and shRanBPM cells, n = 4. Data are presented as mean ± SD. *$P < .05$, **$P < .01$, ns: non-significant (Student's t test)

its degradation, showing the value of not limiting the scope of experiments of E3 ligase substrates to just changes of protein levels. However, the minimal overlap we found between increased proteins and decreased ubiquitination in shRanBPM cells suggests non-degradative ubiquitination regulation by the CTLH complex might be a more common occurrence than previously anticipated. The diGLY data cannot distinguish between mono- and poly-ubiquitination, however, our assessment of PKM2 and LDHA ubiquitination by western blots reveals it to be polyubiquitination. Which E2 enzyme and which ubiquitin linkage type are involved in these ubiquitination events affecting signaling remain an open question. Our observation that recombinant RMND5A can pair with UBE2D2 E2 enzyme to make polyubiquitin chains with K48 and/or K63 linkages in vitro[16] suggests K63 as a possibility. K63-linked polyubiquitination has a wide range of functional outcomes including regulating complex assembly and protein activation.[8]

CTLH complex subunits contain a variety of protein-protein interaction domains that likely are used to recruit specific substrates: muskelin (discoidin and kelch repeat domains), ARMC8 (ARM repeats), RanBPM (SPRY), and WDR26 (WD40 repeats). The architecture of the yeast complex has been elegantly characterized by Qiao et al, 2020 using cryo-EM,[6] however, deviations between the yeast and human complex preclude clear understanding of the positions of the human subunits as substrate receptors in the CTLH complex.[14] Thus, the subunit(s) responsible for recruiting LDHA and PKM2 await future investigation.

Our data indicate that the CTLH complex functions to normally restrict glycolytic flux at least in part by inhibiting the activity levels of PKM2 and LDHA, and potentially also ENO1, via ubiquitination. We observed increased glycolysis and glycolytic capacity in HeLa cells depleted of RanBPM accompanied by changes in related metabolites and nucleotides. The Warburg effect is the metabolic reprogramming that cancer cells exhibit of increased glucose uptake and lactate production even under abundant oxygen.[2] Although not completely understood, increased glycolytic flux supports cell proliferation by several proposed mechanisms, such as rapid ATP synthesis and supporting biosynthetic pathways that branch off from glycolysis intermediates (Figure 4B).[2] Thus, our results suggest that mutation or loss of expression of the CTLH complex could benefit a cancer cell by providing a means to upregulate glycolysis. We previously have shown that loss of RanBPM and RMND5A increases cell proliferation in HEK293 cells and loss of RanBPM promotes tumor development in a xenograft model.[20,24]

This report not only provides a resource for identifying substrates of a newly discovered E3 ligase, but also reveals a novel function of the CTLH complex in glycolysis as a post-translational mechanism needed to keep glycolytic flux at an appropriate level in HeLa cells. We determined that two likely substrates of the complex are PKM2 and LDHA, but, instead of proteasomal degradation, their activity is regulated. It is an overall function of regulating glucose metabolism that is shared by the yeast Gid complex, although on opposing pathways (gluconeogenesis vs glycolysis) and a different mechanism. Cancer cells rely on glycolysis for survival as a quick energy source and supply of intermediates for biosynthetic pathways. Our findings of ubiquitination inhibition at multiple points of the glycolysis pathway may provide an avenue for development of a CTLH complex agonist (eg, small molecule trapping CTLH complex interaction with PKM and/or LDHA) as a future therapeutic strategy for cancer patients once structural elucidation of the human complex is completed.

ACKNOWLEDGMENTS

We thank members of Schild-Poulter and Lajoie laboratories (especially Paula Pittock and Dr Dylan Diesters-Castator) for helpful discussions, technical help, and advice and Zach Easton, Dr Tim Regnault, Fatemeh Mirshafiei Langari, and Dr Sean Cregan for assistance with the Seahorse assay. This work was supported by operating grant MOP-142414 from the Canadian Institutes for Health Research (CIHR) to C.S-P. Mass spectrometry analyses were performed on equipment funded by a grant from the Canada Foundation for Innovation to GAL. MERM was supported by an Ontario Graduate Scholarship (OGS) and a Postgraduate Doctoral scholarship from the Natural Sciences and Engineering Research Council of Canada (NSERC).

CONFLICT OF INTEREST

The authors declare that they have no conflict of interest.

AUTHOR CONTRIBUTIONS

C. Schild-Poulter and GA Lajoie designed research, acquired funding, and edited the manuscript. MER Maitland performed research, analyzed data, and wrote the manuscript. M. Kuljanin and X. Wang performed research.

DATA AVAILABILITY STATEMENT

The mass spectrometry proteomics data have been deposited to the ProteomeXchange Consortium via the PRIDE partner repository with the dataset identifier PXD024872.[55]

ORCID

Caroline Schild-Poulter https://orcid.org/0000-0001-9943-9942

REFERENCES

1. Israelsen WJ, Vander Heiden MG. Pyruvate kinase: function, regulation and role in cancer. *Semin Cell Dev Biol*. 2015;43:43-51.
2. Liberti MV, Locasale JW. The Warburg effect: how does it benefit cancer cells? *Trends Biochem Sci*. 2016;41:211-218.
3. De Berardinis RJ, Chandel NS. Fundamentals of cancer metabolism. *Sci Adv*. 2016;2:e1600200.
4. Pavlova NN, Thompson CB. The emerging hallmarks of cancer metabolism. *Cell Metab*. 2016;23:27-47.
5. Santt O, Pfirrmann T, Braun B, et al. The yeast GID complex, a novel ubiquitin ligase (E3) involved in the regulation of carbohydrate metabolism. *Mol Biol Cell*. 2008;19:3323-3333.
6. Qiao S, Langlois CR, Chrustowicz J, et al. Interconversion between anticipatory and active GID E3 ubiquitin ligase conformations via metabolically driven substrate receptor assembly. *Mol Cell*. 2020;77:150-163.e9.
7. Budhidarmo R, Nakatani Y, Day CL. RINGs hold the key to ubiquitin transfer. *Trends Biochem Sci*. 2012;37:58-65.
8. Yau R, Rape M. The increasing complexity of the ubiquitin code. *Nat Cell Biol*. 2016;18:579-586.
9. Rennie ML, Chaugule VK, Walden H. Modes of allosteric regulation of the ubiquitination machinery. *Curr Opin Struct Biol*. 2020;62:189-196.
10. Senft D, Qi J, Ronai ZA. Ubiquitin ligases in oncogenic transformation and cancer therapy. *Nat Rev Cancer*. 2018;18:69-88.
11. Chaugule VK, Walden H. Specificity and disease in the ubiquitin system. *Biochem Soc Trans*. 2016;44:212-227.
12. Chen SJ, Wu X, Wadas B, Oh JH, Varshavsky A. An N-end rule pathway that recognizes proline and destroys gluconeogenic enzymes. *Science*. 2017;355(6323):eaal3655.
13. Liu H, Pfirrmann T. The Gid-complex: an emerging player in the ubiquitin ligase league. *Biol Chem*. 2019;400:1429-1441.
14. Francis O, Han F, Adams JC. Molecular phylogeny of a RING E3 ubiquitin ligase, conserved in eukaryotic cells and dominated by homologous components, the Muskelin/RanBPM/CTLH complex. *PLoS One*. 2013;8:e75217.
15. Kobayashi N, Yang J, Ueda A, et al. RanBPM, Muskelin, p48EMLP, p44CTLH, and the armadillo-repeat proteins ARMC8α and ARMC8β are components of the CTLH complex. *Gene*. 2007;396:236-247.
16. Maitland MER, Onea G, Chiasson CA, et al. The mammalian CTLH complex is an E3 ubiquitin ligase that targets its subunit muskelin for degradation. *Sci Rep*. 2019;9:9864.
17. Lampert F, Stafa D, Goga A, et al. The multi-subunit GID/CTLH e3 ubiquitin ligase promotes cell proliferation and targets the transcription factor Hbp1 for degradation. *eLife*. 2018;7:1-23.
18. Zhen R, Moo C, Zhao Z, et al. Wdr26 regulates nuclear condensation in developing erythroblasts. *Blood*. 2020;135:208-219.
19. Liu H, Ding J, Köhnlein K, et al. The GID ubiquitin ligase complex is a regulator of AMPK activity and organismal lifespan. *Autophagy*. 2020;16:1618-1634.
20. McTavish CJ, Bérubé-Janzen W, Wang X, et al. Regulation of c-Raf stability through the CTLH complex. *Int J Mol Sci*. 2019;20:934.
21. Salemi LM, Maitland MER, Yefet ER, Schild-Poulter C. Inhibition of HDAC6 activity through interaction with RanBPM and its associated CTLH complex. *BMC Cancer*. 2017;17:460.
22. Huffman N, Palmieri D, Coppola V. The CTLH Complex in cancer cell plasticity. *J Oncol*. 2019;2019:4216750.
23. Salemi LM, Maitland MER, McTavish CJ, Schild-Poulter C. Cell signalling pathway regulation by RanBPM: molecular insights and disease implications. *Open Biol*. 2017;7:170081.
24. Atabakhsh E, Bryce DM, Lefebvre KJ, Schild-Poulter C. RanBPM has proapoptotic activities that regulate cell death pathways in response to DNA damage. *Mol Cancer Res*. 2009;7:1962-1972.
25. Kuljanin M, Dieters-Castator DZ, Hess DA, Postovit L-M, Lajoie GA. Comparison of sample preparation techniques for large-scale proteomics. *Proteomics*. 2017;17:1600337.
26. Udeshi ND, Mertins P, Svinkina T, Carr SA. Large-scale identification of ubiquitination sites by mass spectrometry. *Nat Protoc*. 2013;8:1950-1960.
27. Kaboord B, Smith S, Patel B, Meier S. Enrichment of low-abundant protein targets by immunoprecipitation upstream of mass spectrometry. *Methods Mol Biol*. 2015;1295:135-151.
28. UniProt Consortium. UniProt: a hub for protein information. *Nucleic Acids Res*. 2015;43:D204-D212.
29. Cox J, Mann M. MaxQuant enables high peptide identification rates, individualized p.p.b.-range mass accuracies and proteome-wide protein quantification. *Nat Biotechnol*. 2008;26:1367-1372.
30. Raudvere U, Kolberg L, Kuzmin I, et al. G:Profiler: a web server for functional enrichment analysis and conversions of gene lists (2019 update). *Nucleic Acids Res*. 2019;47:W191-W198.
31. Merico D, Isserlin R, Stueker O, Emili A, Bader GD. Enrichment map: a network-based method for gene-set enrichment visualization and interpretation. *PLoS One*. 2010;5:e13984.
32. Kucera M, Isserlin R, Arkhangorodsky A, Bader GD. AutoAnnotate: a Cytoscape app for summarizing networks with semantic annotations. *F1000Research*. 2016;5:1717.
33. Shannon P, Markiel A, Ozier O, et al. Cytoscape: a software environment for integrated models of biomolecular interaction networks. *Genome Res*. 2003;13:2498-2504.
34. Reimand J, Isserlin R, Voisin V, et al. Pathway enrichment analysis and visualization of omics data using g:Profiler, GSEA, Cytoscape and EnrichmentMap. *Nat Protoc*. 2019;14:482-517.
35. Atabakhsh E, Wang JH, Wang X, Carter DE, Schild-Poulter C. RanBPM expression regulates transcriptional pathways involved in development and tumorigenesis. *Am J Cancer Res*. 2012;2:549-565.

36. Foerster S, Kacprowski T, Dhople VM, et al. Characterization of the EGFR interactome reveals associated protein complex networks and intracellular receptor dynamics. *Proteomics*. 2013;13:3131-3144.
37. Woo JA, Liu T, Zhao X, et al. Enhanced tau pathology via RanBP9 and Hsp90/Hsc70 chaperone complexes. *Hum Mol Genet*. 2017;26:3973-3988.
38. Soliman SHA, Stark AE, Gardner ML, et al. Tagging enhances histochemical and biochemical detection of Ran Binding Protein 9 in vivo and reveals its interaction with Nucleolin. *Sci Rep*. 2020;10:1-11.
39. Hosono K, Noda S, Shimizu A, et al. YPEL5 protein of the YPEL gene family is involved in the cell cycle progression by interacting with two distinct proteins RanBPM and RanBP10. *Genomics*. 2010;96:102-111.
40. Fan J, Hitosugi T, Chung T-W, et al. Tyrosine phosphorylation of lactate dehydrogenase A is important for NADH/NAD+ redox homeostasis in cancer cells. *Mol Cell Biol*. 2011;31:4938-4950.
41. Liu K, Li F, Han H, et al. Parkin regulates the activity of pyruvate kinase M2. *J Biol Chem*. 2016;291:10307-10317.
42. Dong C, Zhang H, Li L, Tempel W, Loppnau P, Min J. Molecular basis of GID4-mediated recognition of degrons for the Pro/N-end rule pathway article. *Nat Chem Biol*. 2018;14:466-473.
43. Dong C, Chen SJ, Melnykov A, et al. Recognition of nonproline N-terminal residues by the Pro/N-degron pathway. *Proc Natl Acad Sci U SA*. 2020;117:14158-14167.
44. Cairns RA, Harris IS, Mak TW. Regulation of cancer cell metabolism. *Nat Rev Cancer*. 2011;11:85-95.
45. Lv L, Li D, Zhao D, et al. Acetylation targets the M2 isoform of pyruvate kinase for degradation through chaperone-mediated autophagy and promotes tumor growth. *Mol Cell*. 2011;42:719-730.
46. Ventura M, Mateo F, Serratosa J, et al. Nuclear translocation of glyceraldehyde-3-phosphate dehydrogenase is regulated by acetylation. *Int J Biochem Cell Biol*. 2010;42:1672-1680.
47. Huang H, Tang S, Ji M, et al. p300-Mediated lysine 2-hydroxyisobutyrylation regulates glycolysis. *Mol Cell*. 2018;70:663-678.e6.
48. Goto T, Matsuzawa J, Iemura SI, Natsume T, Shibuya H. WDR26 is a new partner of Axin1 in the canonical Wnt signaling pathway. *FEBS Lett*. 2016;590:1291-1303.
49. Puverel S, Barrick C, Dolci S, Coppola V, Tessarollo L. RanBPM is essential for mouse spermatogenesis and oogenesis. *Development*. 2011;138:2511-2521.
50. Wei Q, Boulais PE, Zhang D, Pinho S, Tanaka M, Frenette PS. Maea expressed by macrophages, but not erythroblasts, maintains postnatal murine bone marrow erythroblastic islands. *Blood*. 2019;133:1222-1232.
51. Heisler FF, Pechmann Y, Wieser I, et al. Muskelin coordinates PrPC lysosome versus exosome targeting and impacts prion disease progression. *Neuron*. 2018;99:1155-1169.e9.
52. Lakshmana MK, Yoon IS, Chen E, Bianchi E, Koo EH, Kang DE. Novel role of RanBP9 in BACE1 processing of amyloid precursor protein and amyloid β peptide generation. *J Biol Chem*. 2009;284:11863-11872.
53. Cao WX, Kabelitz S, Gupta M, et al. Precise temporal regulation of post-transcriptional repressors is required for an orderly drosophila maternal-to-zygotic transition. *Cell Rep*. 2020;31:107783.
54. Zavortink M, Rutt LN, Dzitoyeva S, et al. The E2 Marie Kondo and the CTLH E3 ligase clear deposited RNA binding proteins during the maternal-to-zygotic transition. *eLife*. 2020;9:1-48.
55. Perez-Riverol Y, Csordas A, Bai J, et al. The PRIDE database and related tools and resources in 2019: improving support for quantification data. *Nucleic Acids Res*. 2019;47:D442-D450.

SUPPORTING INFORMATION

Additional supporting information may be found online in the Supporting Information section.

How to cite this article: Maitland MER, Kuljanin M, Wang X, Lajoie GA, Schild-Poulter C. Proteomic analysis of ubiquitination substrates reveals a CTLH E3 ligase complex-dependent regulation of glycolysis. *FASEB J*. 2021;35:e21825. https://doi.org/10.1096/fj.202100664R